JACS
JOURNAL OF THE AMERICAN CHEMICAL SOCIETY
Article
pubs.acs.org/JACS

Patchy Particle Packing under Electric Fields

Pengcheng Song,[†] Yufeng Wang,[†,‡] Yu Wang,[†] Andrew D. Hollingsworth,[‡] Marcus Weck,*[,†] David J. Pine,*[,‡] and Michael D. Ward*[,†]

[†]Molecular Design Institute and Department of Chemistry, New York University, New York, New York 10003, United States
[‡]Center for Soft Matter Research and Department of Physics, New York University, New York, New York 10003, United States

Supporting Information

ABSTRACT: Colloidal particles equipped with two, three, or four negatively charged patches, which endow the particles with 2-fold, 3-fold, or tetrahedral symmetries, form 1D chains, 2D layers, and 3D packings when polarized by an AC electric field. Two-patch particles, with two patches on opposite sides of the particle (2-fold symmetry) pack into the *cmm* plane group and 3D packings with *I*4*mm* space group symmetry, in contrast to uncharged spherical or ellipsoidal colloids that typically crystallize into a face-centered ABC layer packing. Three-patch particles (3-fold symmetry) form chains having a 2_1 screw axis symmetry, but these chains pair in a manner such that each individual chain has one-fold symmetry but the pair has 2_1 screw axis symmetry, in an arrangement that aligns the patches that would favor Coulombic interactions along the chain. Surprisingly, some chain pairs form unanticipated double-helix regions that result from mutual twisting of the chains about each other, illustrating a kind of polymorphism that may be associated with nucleation from short chain pairs. Larger 2D domains of the three-patch particles crystallize in the *p*6*m* plane group with alignment (with respect to the field) and packing densities that suggest random disorder in the domains, whereas four-patch particles form 2D domains in which close-packed rows are aligned with the field.

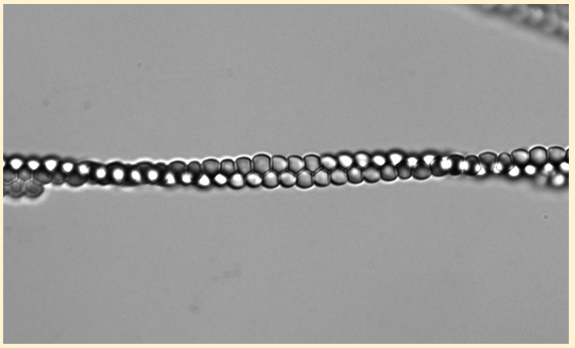

INTRODUCTION

During the past decade, reports have described the synthesis of colloidal particles shaped as cubes,[1] rods, ellipsoids, triangles, clusters of spheres,[2−4] and dimpled particles.[5−8] The simple symmetry of these particles has largely limited three-dimensional (3D) packing to face-centered and body-centered cubic structures.[9] The formation of noncubic structures has been reported for colloidal alloys,[10−12] but more complex packings that access a larger fraction of the 230 available space groups and 17 plane groups in molecular crystals remain a challenge. Our laboratory recently reported that colloidal particles with shapes of planar organic polyacenes could pack in 2D plane groups that mimicked layer packing in molecular crystals,[13] but the crystallization of most molecules is determined by their charge distribution, which typically is nonuniform. For example, xenon difluoride (XeF_2), a linear molecule with partial negative charge at both ends, crystallizes in the *I*4 *mmm* space group, a body-centered structure, instead of $P6_3/mmc$, even though the latter would be expected to have a higher packing fraction.[14] Organic molecules also form complex hierarchical assemblies, no better exemplified than by the DNA double helix, which forms as a consequence of directional intermolecular interactions.

Colloidal particles with unique symmetries that mimic molecular valence can be realized by site-specific modification with functional groups that create "patches".[15−17] For example, Janus particles can be created through introduction of a single patch on the surface of a colloidal particle,[18−20] while triblock Janus particles equipped with two patches can be fabricated by glancing-angle deposition, and assembled into a Kagome lattice.[21] We recently reported particles with varying numbers of sticky patches, arranged such that the particles mimicked the valency of atoms with monovalent s or p orbitals and multivalent sp, sp^2, sp^3, sp^3d, sp^3d^2, and sp^3d^3 hybridized orbitals to form assemblies akin to molecules.[22] Large-scale structures based on this concept of molecular valency have yet to be produced, however.

Control of patchy particle organization, motion, and interactions using electric and magnetic fields has been reported.[23−26] Upon application of an electric field, the surface charge of patchy particles redistributes in response to the external electric field. In a nonuniform electric field, a dielectrophoretic (DEP) force can either concentrate particles into a region of maximum field strength (positive DEP) or repel them from that region (negative DEP), depending on the relative dielectric constants of the particles and medium.[27] The DEP force depends on the magnitude of the electric field (actually the square of *E*) and the gradient of the field. DEP is independent of field direction, allowing the use of AC fields.

Herein, we report the crystallization of colloidal particles, prepared with charged patches, which mimic molecules with

Received: December 16, 2014
Published: February 18, 2015

DOI: 10.1021/ja5127903
J. Am. Chem. Soc. 2015, 137, 3069−3075

valence and form various packings under the influence of an AC electric field. Colloidal particles with two, three, and four negatively charged patches endow the particles with 2-fold, 3-fold, or tetrahedral symmetries. Whereas "two-patch" particles with 2-fold symmetry crystallize in the *I*4 *mm* space group, a body-centered lattice with an ABA layer structure that mimics the crystal structure of XeF_2. Three-patch particles form chains having a 2_1 screw axis symmetry, but these chains pair in a manner such that each individual chain has one-fold symmetry but the pair has 2_1 screw axis symmetry, in an arrangement that aligns the patches that would favor Coulombic interactions along the chain. Surprisingly, some chain pairs form unanticipated double-helix regions that result from mutual twisting of the chains about each other, illustrating a kind of polymorphism that may be associated with nucleation from short chain pairs.

METHODS

Patchy Particles Fabrication. Patchy particles were fabricated following the cluster-encapsulation method.[3,22] Sulfonated polystyrene microspheres (850 nm in diameter, 3% divinylbenzene cross-linked) with negatively charged surfaces were synthesized by surfactant-free emulsion polymerization, using potassium persulfate (KPS) as an initiator, which introduced sulfonate groups on the microsphere surface. An "emulsion-evaporation" method was used to create small clusters of the microspheres,[3] which were then swollen and encapsulated by a specified amount of styrene. The styrene was then polymerized through free radical polymerization using benzoyl peroxide initiator[3] to produce the patchy particles. Sodium dodecyl sulfate (SDS) was used as surfactant in both the cluster and patchy particle formation steps. Density gradient centrifugation was employed to separate the patchy particles into discrete groupings according to the number of microspheres, as described previously.[3] The patchy particles were washed by centrifugation/redispersion three times with deionized water to remove residual SDS (surfactants are not required because the sulfonate groups on the patches stabilize the particles against aggregation). After the final wash, the particles of interest were diluted to 0.2% (v/v) for use in crystallization experiments.

Patchy Particles Crystallization. Crystallization of the patchy particles was investigated in a dielectrophoretic cell (Figure S1, Supporting Information), fabricated by successive thermal evaporation of chromium (5 nm thick, adhesion layer) and gold (70 nm thick) on a glass microscope slide using a rectangular glass tube (variable 0.5 to 0.7 mm, VitroCom, Mountain Lakes, NJ, USA) as a mask to create two rectangular electrodes separated by a gap. A copper lead (0.5 mm diameter) was attached to each electrode with silver paint (SPI Paint, West Chester, PA). The crystallization container was fabricated by affixing glass coverslips (No. 0, 110 μm thick, Corning Incorporated, Corning, NY, USA), which served as spacers, to the electrode-patterned glass slide with a UV curable, thiolene-based adhesive (NOA 72, Norland Products) followed by curing under UV (360 nm) for 60 s. A second coverslip (No. 2, 180 μm thick) was attached to the top surfaces of the spacers, thereby creating a rectangular volume for the colloidal particle suspension. The cell was filled with a particle suspension (0.2% by volume in water) of the desired particles to ensure that 30% of the bottom surface of the cell was covered. The cell was sealed with UV-curable adhesive (cured under UV irradiation (360 nm) for 2 min) and allowed to stand for 12 h in a horizontal position, thereby allowing the particles (density, 1.05 g/cm^3) to settle at the bottom of the cell. The gravitational height of the individual patchy particles is approximately 4 μm.

The two copper leads of the dielectrophoretic cell were connected to the output side of a voltage amplifier (10×) with a 1 μF capacitor installed on one of the leads to eliminate residual parasitic DC current in the circuit. A function generator was connected to the input side of the amplifier. The frequency of the AC electric field used was in the range 5 kHz $\leq f \leq$ 500 kHz and the field strength 100 V/cm $\leq E \leq$ 500 V/cm. Field strengths and frequencies in these ranges were sufficient to mobilize the particles under dielectrophoresis (DEP), driving the particles, with a lower dielectric constant (ε = 2.6) relative to the aqueous medium (ε = 78.5), to the region of lowest field strength, which is in the center of the cell between the two electrodes and away from the energized surface (negative DEP; see Figure S1, Supporting Information).

The packing of the colloidal particles was characterized using a custom-built laser diffraction apparatus. Unlike optical microscopy, which is confined to a local field of view, diffraction of an incident laser beam can provide structural information averaged over a larger area. A green laser source (λ = 532 nm, 50 mW power output, Weiita Corp, NJ) was attached to the top of a supporting stand. (Caution! Strong laser beam and its reflection may injure eyes. Laser protection goggles are required for operation.) A microscope stage (Leica, Germany), used as the sample holder, was placed 30 cm beneath the laser generator. A beam stop was installed 10 cm below the microscope stage to block the central laser beam. The diffraction pattern was projected onto a reflector constructed from a flat board covered by grid-printed paper. The distance between the sample and reflector was adjusted from 25 to 30 cm to accommodate scattering from two-, three-, or four-patch particles. A DSLR camera (5D Mark III, Canon, Japan) was used to record the diffraction pattern. The laser was turned on only while recording to prevent heating of the sample.

The symmetry and *d*-spacings in colloidal crystals were determined from the Fraunhofer diffraction equation (eq 1), where *P* is the distance between the central spot on the diffraction pattern and each laser spot on the reflector, D_F is the sample-to-reflector distance, λ is the laser wavelength, and *n* is an integer corresponding to the order of diffraction (Figure S2, Supporting Information).

$$\sin\theta = \frac{n\lambda}{d};\ \theta = \tan^{-1}\frac{P}{D_F} \quad (1)$$

Particle Models. Packing densities of the close-packed hexagonal arrays of the three-patch particles were calculated with AutoCAD (AutoDesk, Inc.), beginning with loosely packing *p6m* lattice of replicas of the three-patch particles, followed by compression until the edges of each particle contacted six neighbors while maintaining *p6m* symmetry. Particle chain models also were constructed with AutoCAD.

RESULTS AND DISCUSSION

Patchy particles were synthesized following a procedure previously reported by our laboratory (Figure 1).[22] Scanning electron microscopy (SEM) verified the number of patches, their disposition on the microsphere surface, and the particle dimensions. The length and width of a typical two-patch

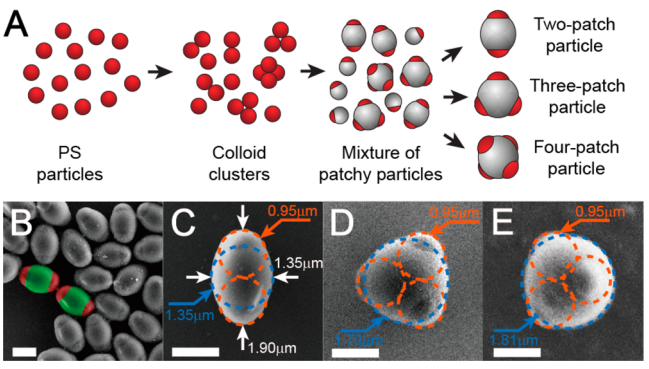

Figure 1. Fabrication and SEM images of patchy particles. (A) Fabrication process of patchy particles. (B) SEM images of two-patch particles. The patches of two particles are colored red and their matrix parts green. SEM image of (C) two-, (D) three-, and (E) four-patch particles. The matrix and patches are labeled with blue and orange dashed lines. Scale bar = 1 μm.

DOI: 10.1021/ja5127903
J. Am. Chem. Soc. 2015, 137, 3069−3075

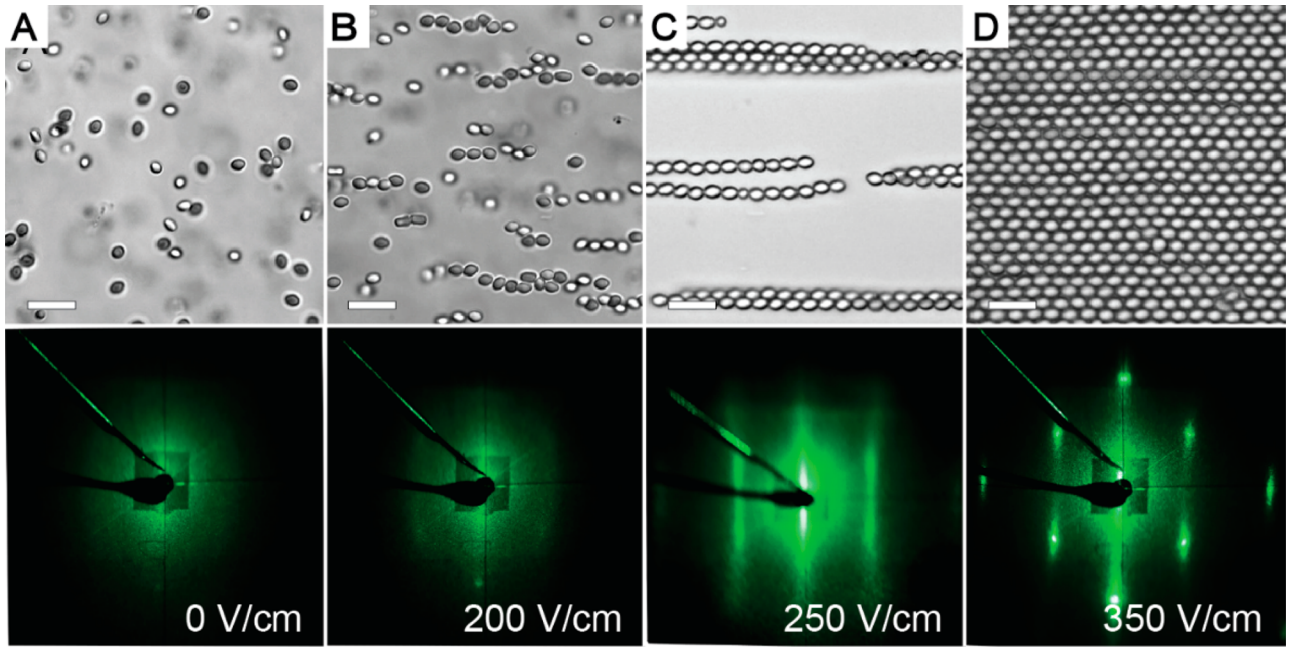

Figure 2. Optical microscopy images of two-patch particles at electric field strengths of (A) 0, (B) 200, (C) 250, and (D) 350 V/cm (upper). $f = 100$ kHz. Laser diffraction patterns under the same conditions (lower). Scale bar = 6 μm.

particle were 1.90 and 1.35 μm, respectively (Figure 1C). A typical three-patch particle had an inner matrix diameter of 1.70 μm with 0.95 μm diameter patches (Figure 1D), and a typical four-patch particle had an inner matrix diameter of 1.81 μm with 0.95 μm diameter patches (Figure 1E). The cross-sectional diameter of the patches was 0.95 μm for all particles, regardless of the number of patches.

The interaction between two patchy particles, with a neutral matrix and negatively charged patches, differs from that of noncharged or charged spherical particles. The Coulomb forces between two charged colloidal particles in an aqueous solution is modified by the medium. According to DLVO theory, the force between two charged spherical particles immersed in a liquid is approximated by

$$F(D) = \frac{2\pi\sigma^2 R}{\varepsilon\varepsilon_0\kappa} e^{-\kappa D} - \frac{AR}{12D^2} \tag{2}$$

where σ is the surface charging density of the particle, R is the radius of the particle, D is the distance between two particles, ε is the dielectric constant of the medium, ε_0 is the permittivity of free space, A is the Hamaker constant, and κ^{-1} is the Debye screening length, the characteristic distance over which electrostatic effects decay. Progress toward modeling of more complicated interactions, for example, between "inverse patchy colloids" consisting of negatively charged spherical particles carrying a small number of positively charged patches on opposite poles, has been reported.[28] Detailed modeling of this kind for the two- and three-patch particles described here is beyond the scope of this contribution, however.

When D is much larger than κ^{-1}, the electrostatic interaction between the two particles is screened. For spherical particles at room temperature κ^{-1} can be approximated by

$$\kappa^{-1} = \frac{0.304}{z\sqrt{c_0[M]}} \tag{3}$$

where the ionic valence z is 1 and the ionic strength c_0 in deionized water is in the range 10^{-4} to 10^{-5} M, yielding $30 \leq \kappa^{-1} \leq 96$ nm. To compare this length scale with an n-patch particle size, we assumed an equivalent radius, $n^{1/3}R$, where R is the constituent sphere radius.

In the case of patchy particles, the effect of surface charge density on the patches, q, must be considered. Assuming all the KPS initiator used in the emulsion polymerization is incorporated into the surface of the polystyrene particles and each sulfonate group is ionized, the estimated charge density is -10 μC/cm^2 (see the Supporting Information). This value is about 5 to 10 times higher than reported for sulfate-terminated polystyrene colloids. Assuming $q = -1$ μC/cm^2 for the constituent spheres, electrophoretic mobility measurements on patchy particles indicated that a significant portion of the sulfonate groups are buried within the uncharged polystyrene matrix. The measured values for two- and three-patch particles were -0.078 and -0.062 μC/cm^2, respectively. Although the corresponding ζ potentials were small (≈ -15 mV), position tracing with optical microscopy of two two-patch particles in an aqueous suspension (no applied E field) revealed that the particles repelled each other at close approach. This behavior can be attributed to the negative charge on the patches and adsorbed anionic surfactant.

In the presence of an electric field, the observed particle assemblies can be explained in terms of a combination of attractive dipolar interparticle interactions and the expulsion of patchy particles from regions of maximum field intensity.[29,30] A detailed description of the polarization mechanisms for polystyrene spheres in water has been reported.[27] The sign and magnitude of the induced dipoles in the colloids are determined by the real part of the Clausius−Mossotti function, $Re\{K^*(\omega)\}$ (see the Supporting Information). Using the measured values of q, as well as dielectric constants and conductivities corresponding to the particles and medium, the DEP force is always negative in the experiments described herein. The dipolar chaining force is always positive and

DOI: 10.1021/ja5127903
J. Am. Chem. Soc. 2015, 137, 3069−3075

attractive, and it is estimated to be 20−40 k_BT at the electrode surface. Although the electric field was not computed, we note that the gravitational energy of micron diameter PS particles in water 70 μm above a surface (40 μm below the microscope coverslip in our cell) is on the order of 10 k_BT. Furthermore, the relative energy of the dipole−dipole and DEP effects is $\Phi_{DEP}/\Phi_{DD} = 2/Re\{K^*(\omega)\} \approx -5$, suggesting that the chaining force was weaker but sufficient for particle structuring at higher number densities. Notably, the elongated (e.g., ellipsoidal) dielectric particles typically respond to an E field by aligning with their long axes parallel to the field vector.

Accordingly, the negative DEP force concentrates the patchy particles in the center of the cell above the electrodes where the field strength is lower, thereby densifying the particle suspension and inducing organization into large-scale structures, which are visible in both microscope images and laser diffraction patterns (Figure 2). The size of the spherical spot on the laser diffraction pattern is inversely proportional to the size of a two-patch particle (Figure 2A). Upon increasing the electric field strength to 200 V/cm, the negative charges on one of the patches are neutralized by the polarizing surface charges and the negative charges on the opposite patch are strengthened: the particles begin to form pairs or short chains in the direction of electric field, which assemble and disassemble dynamically. The laser diffraction pattern exhibits four faint spots that correspond to an interparticle separation of $d = 2.1 \pm 0.03$ μm between two particles in an isolated pair or between particles in a short chain (Figure 2C,D; standard deviation in Figure 2B is 0.09 μm). This value compares favorably with the size of the particles measured by scanning electron microscopy (1.95 ± 0.04 μm).

Increasing the electric field strength to E = 250 V/cm produces chains containing dozens of two-patch particles as well as small rafts consisting of a few chains, as depicted in Figure 2C. The association of chains in the rafts was reversible. Diffraction associated with the interchain distances was not sufficiently coherent for analysis, but the three bright strips on the diffraction pattern corresponded to the interparticle distance within each chain (Figure 2C). In addition, large-scale ordered arrays of two-patch particles were formed in the center of the cell due to the dielectrophoretic (DEP) force. Typically, the chains formed within 1−3 min whereas the rafts formed within 5−20 min, and the patchy particles formed less quickly than uncharged spherical polystyrene particles. A well-defined laser diffraction pattern was observed at E = 350 V/cm and optical microscopy revealed a close-packed arrangement of two-patch particles (Figure 2D). These data were consistent with packing in the *cmm* plane group, which is characterized by two unique 2-fold rotation axes and two mirror planes (Figure 3). The laser diffraction pattern is consistent with the lattice parameters a = 2.09 μm and b = 2.54 μm (Figure 3B).

We note that the DEP force responsible for driving particle packing depended on the combination of the strength and frequency of the electric field. The packing of the two-patch particles at various electric field strengths of 250, 300, and 350 V/cm was compared at 10 and 100 kHz (Figure S5, Supporting Information). At a given frequency, particles assembled into chains parallel to the electric field at these field strengths, but at lower field strengths the interchain ordering tended to decrease. In general, the particle packing expanded both parallel and perpendicular to the chains when the electric field strength was decreased. This expansion was larger at 10 kHz than at 100 kHz, yet the peaks from the FFT associated with the interchain

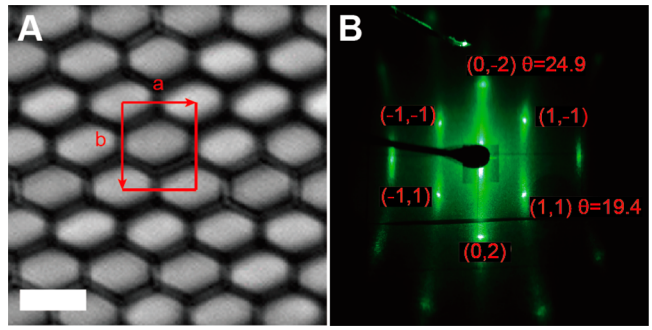

Figure 3. Packing of two-patch particles at E = 350 V/cm and f = 100 kHz. (A) Optical microscopy image of a single layer of two-patch particles in the *cmm* plane group. (B) Laser diffraction pattern of the packing in panel A, with diffraction spots corresponding to d = 1.60 μm (1,1) and d = 1.26 μm (0,2). The spot corresponding to (0,1) is absent by symmetry. Scale bar = 2 μm.

distances under 10 kHz typically were sharper than at 100 kHz for a given field strength, suggesting that interchain ordering was greater at the lower frequency.

Colloidal crystals containing more than one layer of two-patch particles were formed by increasing the initial particle concentration from 0.2% (v/v) to 0.4% (v/v) and increasing the electric field strength to E = 500 V/cm at f = 100 kHz (Figure 4). Microscopy images of the layer packing of the two-patch particles in multilayered structures were obtained by adjusting the focal plane on each layer. The packing in each layer was *cmm*, with each layer translated with respect to the adjacent layer by **b**/**2** (Figure 4A,B). In contrast to the packing

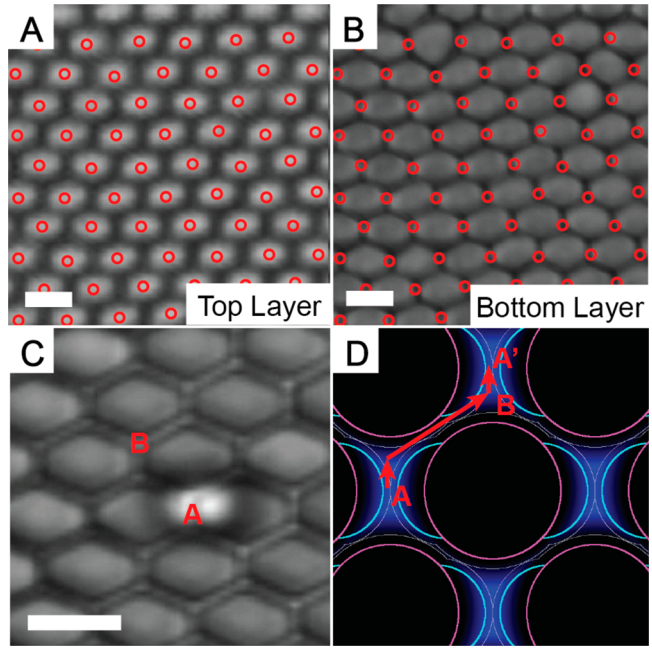

Figure 4. Multilayer packing of two-patch particles at E = 500 V/cm and f = 100 kHz. (A) Optical microscopy image of the top layer of a double-layer structure with two-patch particles. (B) Microscopy image of the bottom layer. Red circles show the position of two-patch particles in the top layer. (C) Microscopy image of a two-patch particle docking on top of a layer of packed two-patched particles. (D) Calculated docking energy map for panel C by eq 4, where the more intense blue regions correspond to lower (i.e., more favorable) docking energy. Scale bar = 2 μm.

DOI: 10.1021/ja5127903
J. Am. Chem. Soc. 2015, 137, 3069−3075

of noncharged sphere or ellipsoid particles that normally form a face-centered lattice with a ABC layer structure, the two-patch particles adopt an ABA layer structure with a body-centered lattice, *I*4*mm* space group, with parameters of a = 1.51 μm and b = 2.15 μm.

Uncharged ellipsoidal particles in an upper layer would be expected to dock at site **B** in the lower layer in Figure 4C to optimize packing density. In the case of two-patch particles, however, the particles in an upper layer dock on the layer below at site **A** due to the introduction of electric potential energy by the electric field. The potential of a single two-patch particle on either site **A** and **B** can be estimated from the sum of the gravitational energy and electric potential energy

$$E = (\rho_p - \rho_m)V_p gh + \frac{1}{4\pi\varepsilon_0\varepsilon_m}\left(\sum_{i=1}^{n}\frac{q_1 q_i}{r_i} + \sum_{j=1}^{m}\frac{q_2 q_j}{r_j}\right) \quad (4)$$

where ρ_p and ρ_m are the densities of particles and matrix, g is the gravitational constant, h is the height as measured from the center of the particle to the center of the underlying *cmm* layer, q_1 and q_2 are the charges on two patches, r_i and r_j are the distances between patches and the surrounding two-patch particles, and ε_m is the dielectric constant of suspension. A "docking energy map" for a two-patch particle on a *cmm* layer of two-patch particles using eq 4 reveals that the lowest potential energy site is located at site **A** of the bottom layer (Figure 4D) in agreement with observation. The difference in docking energy between sites **A** and **B**, in terms of gravity and electric potential energy, is given by eq 5. The difference in electric potential energy between the two sites is approximately 100 times larger than the difference in gravitational energy. Consequently the electric potential energy dominates the packing behavior of the two-patch particles. Video microscopy of a two-patch particle moving from one docking site to another on a *cmm* layer reveals the two-patch particle shaking on site A and moving along the path A → B→A′, which is calculated to the minimum energy path (Movie S1, Supporting Information).

$$\Delta E = \Delta E_g + \Delta E_e = (-1.3 \times 10^{-22})J + (1.1 \times 10^{-20})J \quad (5)$$

The imposition of a linear AC electric field on the three-patch particles results in behavior different from that of the two-patch particles, as the three-patch particles do not have a unique symmetry-related axis that coincides with the electric field (see Figure S4 in the Supporting Information for SEM images of three-patch particles). The three-patch particles begin to form chains at E = 250 V/cm. The polarization force aligns the chain with the electric field and the DEP force drives the particles to the center of the cell. In the absence of polarization by an electric field, one would expect neighboring particles orient head-to-tail to rotate 90° in order to minimize repulsion between the negatively charged patches. Under and electric field, however, the chains of three-patch particles exhibit segments with a 2_1 screw axis symmetry due to a 180° rotation of successive particles along the chain, as depicted by the chain of 13 three-patch particles in Figure 5A and illustrated by a defect-free segment in Figure 5B. Solid models of a defect-free chain suggest that the 2_1 axial symmetry creates favorable dipole−dipole interactions along the chain between polarized patches when compared with other configurations. Actual

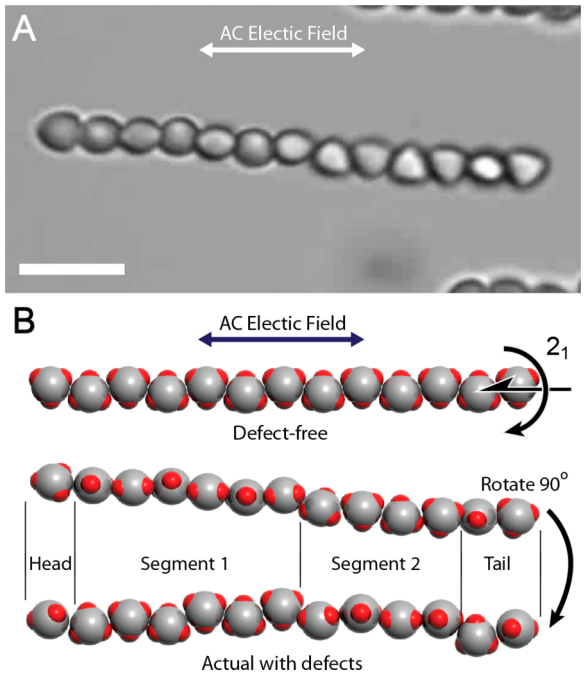

Figure 5. Chains of three-patch particles formed at E = 250 V/cm and f = 100 kHz. (A) Optical microscopy image of a chain containing 13 three-patch particles. Also see Movie S2 in Supporting Information. (B) Model of the chain in panel A, illustrated as an idealized defect-free chain (upper) and a more representative chain (lower) that is separated into two segments by twisting defects. Scale bar = 5 μm.

chains consist of segments interrupted by "defects" associated with a 90° rotation between neighboring particles (Figure 5B).

When three-patch particle chains associate into chain pairs the symmetry of the individual chains changes from the 2-fold helical symmetry to simple one-fold symmetry, but the chain pair can be described as "flat" and packed head-to-head across a 2_1 screw axis that runs along the center of the long axis of the paired chains (Figure 6). This configuration is perhaps not unexpected as it favors strong Coulombic interaction when the patches are polarized along the chain. Surprisingly, some of the paired chains (<5%) display regions in which the chains twist to form a double helix, reflecting a kind of structural polymorphism. There is no statistical preference for left- or right-handed helices. The helical configuration requires that neighboring particles within each chain twist slightly, perhaps reflecting a steric encumbrance between adjacent patches. Double-helix regions complete a 180° turn over a span of 12−13 particles (per chain), suggesting a twist of 15° between neighboring particles. The helical regions can be dynamic, moving along the chain while remaining intact (Figure 6A,B). Some chains exhibit two helical regions separated by a "flat" 2_1 screw axis segment. Chain pairs containing 13 particles and a corresponding 180° twist uncoiled within 10 min upon contacting the substrate surface of the dielectrophoretic cell, fracturing and then reassembling to form uncoiled chain pairs (Figure S3, Supporting Information). Chain pairs consisting of 26 particles with a full 360° twist, as well as long chains that contained two 180° helices separated by a flat 2_1 screw axis segment (e.g., Figure 6A,B), remained coiled when in contact with the substrate for at least 5 h, however. Although the origin of the double helix chains remains undetermined at this time, mature single chains do not pair into a helix configuration. Therefore, it is reasonable to suggest that the double helix

DOI: 10.1021/ja5127903
J. Am. Chem. Soc. 2015, 137, 3069−3075

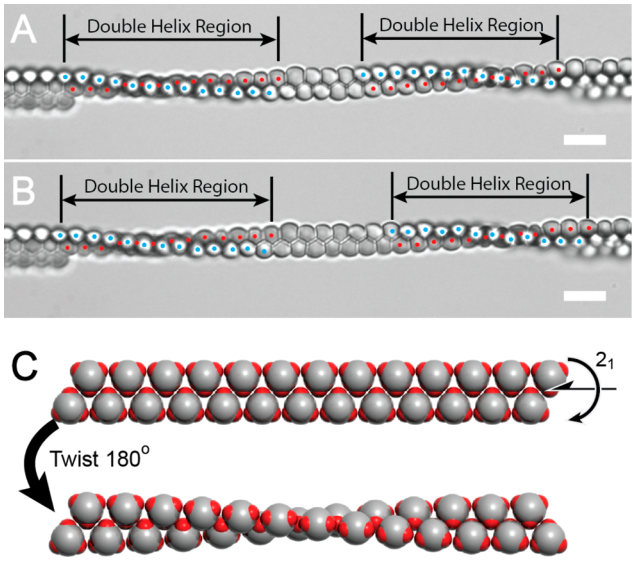

Figure 6. (A) Paired chains of three-patch particles containing two double helix regions formed at E = 250 V/cm and f = 100 kHz. The double helix regions in the two paired chains are denoted by red and blue dots. (B) The same paired chains after 35 s at E = 250 V/cm. (C) Model of a chain pair with 2_1 screw axis along the center of the double chain, with head-to-head packing across the screw axis (upper) and the twist structure of three-patch particles when forming a helix region with a pitch of 13 particles. Scale bars = 5 μm.

emerges from short double chains that become twisted, either momentarily by fluctuations (similar to a nucleation event) or by a torque experienced by a short double chain that is canted with respect to the field. Unfortunately, it was difficult to discern a twist in short double chains.

Assemblies of three-patch particles consisting of more than two chains did not exhibit helical coils. At E = 350 V/cm and f = 100 kHz, multiple chains of three-patch particles eventually assembled into two-dimensional domains consisting of hundreds of particles. The domain packing was consistent with a *p6m* plane group and a lattice parameter of a = 1.94 μm (Figure 7). AutoCAD models based on a *p6m* lattice containing replicas of the three-patch particles suggested closest packing for a unit cell having a lattice parameter a = 1.89 μm, smaller than observed experimentally. Whereas single chains or pairs of chains always oriented with the electric field, the hexagonal

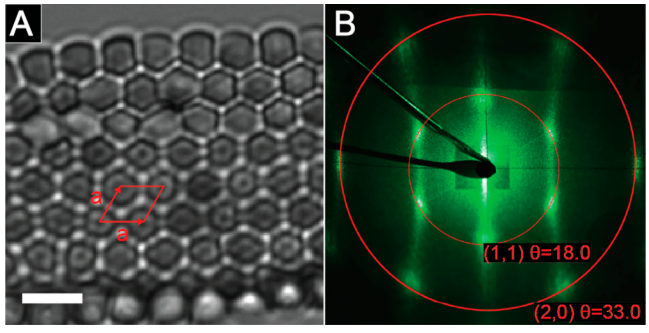

Figure 7. 2D packing of three-patch particles at E = 350 V/cm and f = 100 kHz. (A) Optical microscopy image of a single layer of three-patch particles in the *p6m* plane group. (B) Laser diffraction pattern of the 2D packing in panel A; the spots correspond to d = 1.72 μm (1,1) and d = 0.97 μm (0,2). The diffuse arcs superimposed on the (1,1) spots correspond to various interchain separations. Scale bar = 3 μm.

domains exhibited random orientations with respect to the field. After 1 h of crystallization at E = 350 V/cm, the six (1,1) diffraction spots broadened into small arcs (Figure 8A),

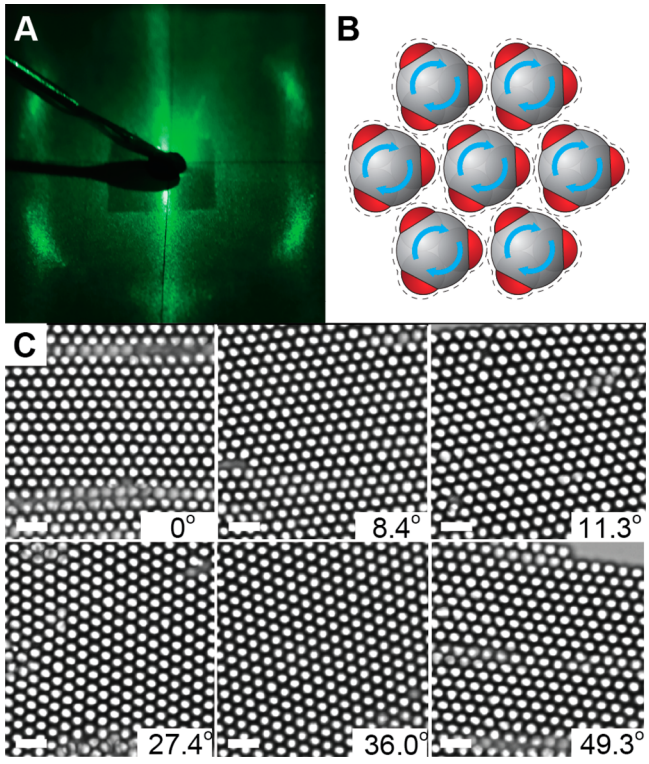

Figure 8. (A) Laser diffraction pattern of a 2D crystal of three-patch particles after 1 h at E = 350 V/cm and f = 100 kHz. The well-defined diffraction spots in Figure 7B have transformed into somewhat broadened arcs, suggesting orientational disorder with respect to the patches. Three-patch particles have freedom of rotation in crystal. (B) Idealized ordered packing of 3-patch particles. (C) Optical microscopy images of three-patch particle domains in different orientations with respect to the electric field, which is oriented horizontally. Scale bar = 5 μm.

suggesting a distribution of interparticle separations owing to orientational disorder of the patches rather than an ordered structure (Figure 8B). This observation is consistent with the random orientation of the islands with respect to the electric field (Figure 8C).

The 2D packing of four-patch particles at E = 350 V/cm and f = 100 kHz conformed to the *p6m* plane group with lattice parameter of a = 2.29 μm (see Figure S4 in the Supporting Information for SEM images of four-patch particles). The diffraction spots are very broad, suggesting a range of interparticle distances, which can be attributed, at least partially, to the presence of two-patch and three-patch impurity particles. The close-packed direction (a axis) of the domains was aligned with the electric field.

CONCLUSION

The observations described above demonstrate that crystallization of patchy particles can be provoked by an electric field and dielectrophoretic forces. Moreover, the polarization produced on the patches by the electric field play an important role in the assembly and alignment of 1D chains, as well as their further assembly into chain pairs, 2D domains, and 3D packings. In the case of two-patch particles the arrangement

DOI: 10.1021/ja5127903
J. Am. Chem. Soc. 2015, 137, 3069−3075

of adjacent layers is contrary to expectations based on close-packing principles and behavior of uncharged elliptical and spherical particles, illustrating the unique influence of polarization and the corresponding dipole forces on colloidal crystal assembly. The observation of double helix regions in chain pairs comprising the three-patch particles is unanticipated and surprising, and it suggests a kind of polymorphism that may be associated with nucleation from short paired chains. Collectively, these observations suggest that electric fields can be used to guide particles with well-defined symmetries into unconventional packing motifs.

■ ASSOCIATED CONTENT

Supporting Information

Experimental procedures and apparatus, supplementary figures, and videos. This material is available free of charge via the Internet at http://pubs.acs.org.

■ AUTHOR INFORMATION

Corresponding Authors

*marcus.weck@nyu.edu (M.W.)
*pine@nyu.edu (D.J.P.)
*mdw3@nyu.edu (M.D.W.)

Notes

The authors declare no competing financial interests.

■ ACKNOWLEDGMENTS

This work was supported primarily by the Materials Research Science and Engineering Center (MRSEC) program of the National Science Foundation under Award Nos. DMR-0820341 and DMR-1420073. The authors also acknowledge support from the MRI program of the National Science Foundation under Award DMR-0923251 for the acquisition of a Zeiss field emission SEM. Additional financial support was provided by NASA (NNX13AR67G) to A.D.H.

■ REFERENCES

(1) Rossi, L.; Sacanna, S.; Irvine, W. T. M.; Chaikin, P. M.; Pine, D. J.; Philipse, A. P. *Soft Matter* **2011**, *7*, 4139−4142.
(2) Meng, G.; Arkus, N.; Brenner, M. P.; Manoharan, V. N. *Science* **2010**, *327*, 560−563.
(3) Manoharan, V. N.; Elsesser, M. T.; Pine, D. J. *Science* **2003**, *301*, 483−487.
(4) Kraft, D. J.; Vlug, W. S.; van Kats, C. M.; van Blaaderen, A.; Imhof, A.; Kegel, W. K. *J. Am. Chem. Soc.* **2008**, *131*, 1182−1186.
(5) Glotzer, S. C.; Solomon, M. J. *Nat. Mater.* **2007**, *6*, 557−562.
(6) Zoldesi, C. I.; van Walree, C. A.; Imhof, A. *Langmuir* **2006**, *22*, 4343−4352.
(7) Sacanna, S.; Irvine, W. T. M.; Chaikin, P. M.; Pine, D. J. *Nature* **2010**, *464*, 575−578.
(8) Sacanna, S.; Pine, D. J. *Curr. Opin. Colloid Interface Sci.* **2011**, *16*, 96−105.
(9) Li, F.; Josephson, D. P.; Stein, A. *Angew. Chem., Int. Ed.* **2011**, *50*, 360−388.
(10) Leunissen, M. E.; et al. *Nature* **2005**, *437*, 235−240.
(11) Macfarlane, R. J.; Lee, B.; Jones, M. R.; Harris, N.; Schatz, G. C.; Mirkin, C. A. *Science* **2011**, *334*, 204−208.
(12) Velikov, K. P.; Christova, C. G.; Dullens, R. P. A.; van Blaaderen, A. *Science* **2002**, *296*, 106−109.
(13) Song, P.; Olmsted, B. K.; Chaikin, P.; Ward, M. D. *Langmuir* **2013**, *29*, 13686−13693.
(14) Packing fractions were determined using the Materials Studio modeling suite (Accelerys, Inc.). Packing fractions for XeF_2: *I4mmm* = 0.80; $P6_3/mmc$ = 0.83.
(15) Glotzer, S. C. *Science* **2004**, *306*, 419−420.
(16) Bianchi, E.; Blaak, R.; Likos, C. N. *Phys. Chem. Chem. Phys.* **2011**, *13*, 6397−6410.
(17) Zhang, Z.; Glotzer, S. C. *Nano Lett.* **2004**, *4*, 1407−1413.
(18) Xu, X.; Rosi, N. L.; Wang, Y.; Huo, F.; Mirkin, C. A. *J. Am. Chem. Soc.* **2006**, *128*, 9286−9287.
(19) Huo, F.; Lytton-Jean, A. K. R.; Mirkin, C. A. *Adv. Mater.* **2006**, *18*, 2304−2306.
(20) Hong, L.; Cacciuto, A.; Luijten, E.; Granick, S. *Langmuir* **2008**, *24*, 621−625.
(21) Chen, Q.; Bae, S. C.; Granick, S. *Nature* **2011**, *469*, 381−384.
(22) Wang, Y.; Wang, Y.; Breed, D. R.; Manoharan, V. N.; Feng, L.; Hollingsworth, A. D.; Weck, M.; Pine, D. J. *Nature* **2012**, *491*, 51−55.
(23) Gangwal, S.; Cayre, O. J.; Velev, O. D. *Langmuir* **2008**, *24*, 13312−13320.
(24) Gangwal, S.; Pawar, A.; Kretzschmar, I.; Velev, O. D. *Soft Matter* **2010**, *6*, 1413−1418.
(25) Ruditskiy, A.; Ren, B.; Kretzschmar, I. *Soft Matter* **2013**, *9*, 9174.
(26) Chaudhary, K.; Juzrez, J. J.; Chen, Q.; Granick, S.; Lewis, J. A. *Soft Matter* **2014**, *10*, 1320.
(27) Mittal, M.; Lele, P. P.; Kaler, E. W.; Furst, E. M. *J. Chem. Phys.* **2008**, *129*, 064513.
(28) Bianchi, E.; Kahl, G.; Likos, C. N. *Soft Matter* **2011**, *7*, 8313−832.
(29) Velev, O. D.; Gangwal, S.; Petsev, D. N. *Annu. Rep. Prog. Chem.* **2009**, *105*, 213−246.
(30) Jones, T. *Electromechanics of Particles*; Cambridge University Press: Cambridge, UK, 1995.

DOI: 10.1021/ja5127903
J. Am. Chem. Soc. 2015, 137, 3069−3075